Chapter 2

Grain-Oriented $Bi_{0.5}Na_{0.5}TiO_3$–$BaZrO_3$ Piezoelectric Ceramics

Ali Hussain and Myong-Ho Kim

Additional information is available at the end of the chapter

http://dx.doi.org/10.5772/62688

Abstract

Piezoelectric ceramics have applications in various electronic devices such as sensors, actuators, energy harvesters, and so on. Most of these devices are manufactured from lead-containing materials because of their excellent electromechanical performance and low cost. However, lead-containing materials are considered as serious threat to the environment and facing restrictions from legislative agencies across the globe. Since last decade, much research efforts have been devoted to produce high-performance lead-free ceramics for industrial applications. Among lead-free candidate materials, bismuth-based perovskite ceramics such as sodium bismuth titanate ($Bi_{0.5}Na_{0.5}TiO_3$, BNT) are considered potential substitute for lead-based materials because of the Bi^{3+} and Pb^{+2} same $6s^2$ lone pair electronic configuration. This chapter describes the synthesis of BNT particles by different techniques; conventional mixed oxide (CMO) route along with topochemical microcrystal conversion (TMC) methods followed by fabrication of $BaZrO_3$-modified BNT ceramics with a chemical composition of $0.994Bi_{0.5}Na_{0.5}TiO_3$–$0.006BaZrO_3$ (BNT–BZ) by a conventional solid-state reaction method, its texture development by reactive templated grain growth method using BNT templates, and comparison of the structural and electromechanical properties of the textured and non-textured counterparts.

Keywords: Perovskite, Piezoelectric, BNT–BZ, Grain orientation, Texture

1. Introduction

Piezoelectricity is a coupling between a material's mechanical and electrical response. In the simple term, when pressure is applied to a piezoelectric material, an electric charge collects on its surface. On the other hand, when field is applied to a piezoelectric material, it mechanically deforms [1]. This behavior of piezoelectric materials is widely utilized in optics, astronomy,

fluid control, and precision machining due to their high generative force, accurate displacement, and rapid response [2, 3].

To date, most of the commonly used piezoelectric materials are lead-based, such as lead zirconate titanate (PZT) and its solid solutions. Lead-containing materials display high piezoelectric coefficients, especially near the morphotrophic phase boundary (MPB) and have dominated the market of piezoelectric industry [1, 4, 5]. However, the hazardous lead content present within these materials raise serious environmental problems. Therefore, environmental issues such as regulations and policies against lead-based materials have been increasingly enacted throughout the world [6–8]. In order to circumvent the drawback of lead toxicity, extensive research is focused on the quest for alternate piezoelectric materials. Numerous research efforts have been devoted to the candidate lead-free piezoelectric materials such as $BaTiO_3$ (BT), $K_{0.5}Na_{0.5}NbO_3$ (KNN), and $Bi_{0.5}Na_{0.5}TiO_3$ (BNT) because of their interesting electromechanical properties. The BT-based ceramics are interesting from the view point of their good ferroelectricity, chemical, and mechanical stability along with easy processing in polycrystalline form [9, 10]; however, they are inadequate for device applications due to their low Curie temperature ($T_c \approx 120°C$) [11, 12]. Alternatively, The $KNbO_3$–$NaNbO_3$ solid solution or the $(K,Na)NbO_3$ (KNN)-based material exhibits good piezoelectric properties as well as high $T_c \approx 420°C$ and have been studied as substitutes for PZT-based ceramics [13–16]. Nevertheless, alkali metal elements present in KNN-based ceramics easily evaporate at high temperatures. Moreover, KNN ceramics are not only hygroscopic but also make transition between orthorhombic and tetragonal structure ($T_{O–T}$) around 200°C, and this transition temperature shifts toward room temperature (RT) with change in composition through doping or substituting other element, which hinders KNN-based ceramics from practical applications [17, 18]. As one of the most feasible lead-free candidates, BNT-based solid solutions have good piezoelectric properties, excellent reproducibility, and high maximum dielectric constant temperature (T_m 300°C) [19–22]. However, poling of pure BNT ceramics is difficult due to their large coercive field (E_c ~ 73 kV/cm), which is overcome by certain amount through compositional modification and texture development [22–25].

In the recent years, extraordinarily large strain has been reported in compositionally designed BNT-based ceramics [20, 21, 26, 27], which seems to be alternative for PZT in specific actuator applications. Beside, compositional design, texture engineering of polycrystalline ceramics is inimitable and vibrant approach to enhance the piezoelectric properties of ceramics without any major change in the base compositions. Several texture development techniques, such as templated grain growth (TGG) [28], reactive TGG (RTGG) [18], oriented consolidation of anisometric particles [29], screen printing [30], multilayer grain growth [31], and directional solidification technology [32], have been employed to improve the electromechanical properties of piezoelectric ceramics. Among all these techniques, RTGG is more suitable for the texture development of perovskite-type materials [33, 34]. In this process, the plate-like template particles that have specific microstructure and crystallographic characteristics are oriented in a matrix ceramic powder through a tape-casting process, and then the consequent heat treatment results in the nucleation and growth of desired crystals on aligned template particles to bring into being textured ceramics [35]. Because of the grain orientation effect

http://dx.doi.org/10.5772/62688

induced by templates particles through RTGG process, textured ceramic samples can be more easily poled and thus deliver much higher dielectric and piezoelectric response in comparison with non-textured counterparts prepared by a conventional mixed oxide (CMO) routes [18, 33, 34].

For texture development of BNT-based ceramics, simple BNT templates are considered the most promising because of their large size and plate-like nature. Nevertheless, BNT templates prepared by CMO route have equiaxial morphology which cannot satisfy the requirement as seed in the RTGG process. An alternative convenient approach is to synthesize plate-like perovskite templates by a topochemical microcrystal conversion (TMC) process. This process involves substitution or modification of the interlayer cations, however, retaining the structural and morphological features of plate-like layered-perovskite precursors by ion exchange and intercalation reactions at low temperatures [36, 37]. Considering the importance of BNT-based ceramics, this chapter describes the synthesis of BNT particles by different techniques; CMO route along with TMC methods followed by fabrication of $BaZrO_3$-modified BNT ceramics with a chemical composition of $0.994Bi_{0.5}Na_{0.5}TiO_3$–$0.006BaZrO_3$ (BNT–BZ) by a conventional solid-state reaction method, its texture development by RTGG method using BNT templates, and comparison of the structural and electromechanical properties of the textured and non-textured BNT-BZ ceramics.

2. Experimental

Reagent-grade metal oxide powders of Bi_2O_3, TiO_2, and Na_2CO_3 (purity >99.9%) were used as starting materials to produce plate-like $Bi_{4.5}Na_{0.5}Ti_4O_{15}$ (BNT4) precursors by molten salt synthesis (MSS) [38]. The stoichiometric amount of the raw BNT4 powder mixture was first mixed with NaCl (99.95%) in a weight ratio of 1:1.5 and then ball milled in polyethylene jar for 24 h. Consequently, the balls were removed and the slurry was dried and then brought to a firmly covered Al_2O_3 crucible for heat treatment at 1100°C for 4 h. The reaction was assumed complete in accordance with the chemical Eq. (1); the NaCl salt was washed away from the as-synthesized product thorough hot de-ionized water. BNT4 platelets, Na_2CO_3, and TiO_2 were then further weighed to provide a total BNT composition in accordance with the chemical Eq. (2). NaCl salt was again added to the powder mixture with 1:1.5 weight ratios, and then milling was carried out in the presence of ethanol through a magnetic stirrer for 5 h. Subsequently, the slurry was dried and a heat treatment at 950°C for 4 h was performed in a firmly covered Al_2O_3 crucible. Finally, NaCl salt was removed through hot de-ionized water from the product and HCl was utilized to remove the bismuth oxide (Bi_2O_3) by-products. For comparison, BNT particles were also produced by CMO route [39].

$$2.25Bi_2O_3 + 0.25Na_2CO_3 + 4TiO_2 \rightarrow Bi_{4.5}Na_{0.5}Ti_4O_{15} + 0.5CO_2 \quad (1)$$

$$Bi_{4.5}Na_{0.5}Ti_4O_{15} + 2Na_2CO_3 + 5TiO_2 \rightarrow 9Bi_{0.5}Na_{0.5}TiO_3 + 2CO_2 \quad (2)$$

Grain-oriented ceramics with a composition of $0.994Bi_{0.5}Na_{0.5}TiO_3$–$0.006BaZrO_3$ (BNT–BZ) were fabricated through RTGG process utilizing the as-synthesized BNT templates [38]. Commercially accessible carbonate powders such as: Na_2CO_3 and $BaCO_3$ (99.95%, Sigma Aldrich) along with metal oxide powders such as: Bi_2O_3, TiO_2, and ZrO_2 (99.9% Junsei Co., Limited) were first weighed according to the stoichiometric formula of BNT–BZ and then mixed by ball milling for 24 h at 250 rpm. The slurry was dried and then calcined at 850°C for 2 h to form a perovskite phase. The as-prepared calcined powders of BNT–BZ were mixed thoroughly with a solvent (60 vol.% ethanol and 40 vol.% methyl-ethyl-ketone, MEK) and triethyl phosphate (dispersant) in a ball mill for 24 h. Subsequently, polyvinyl butyral (binder) and polyethylene glycol/diethyl-ophthalate (plasticizer) were added to the mixtures and the milling was continued again for another 24 h. BNT templates of 15 wt% were then added to the mixture and ball milled with a slow rotation for another 12 h to form a slurry for tape casting. The viscous slurry was tape cast to form a green sheet with a thickness of ~100 μm on a SiO_2-coated polyethylene film by a doctor blade apparatus. Afterward drying, a single layer sheet was cut, laminated, and hot-pressed at a temperature of 45°C and a pressure of 50 MPa for 2 min to form a 2-mm-thick green compact. The compacts were further cut into small samples of about 1 × 1 cm^2 and then heated at 600°C for 12 h with intermediated steps of 250 and 350°C for 6 and 8 h and to remove organic substances prior to sintering. The samples were sintered at 1150°C for 15 h in air atmosphere and were then brought to room temperature at cooling rate of 5°C/min. For comparison, non-textured BNT–BZ ceramics were also prepared through conventional solid-state reaction [38].

Crystalline phase and purity information of the as-synthesized BNT particles and BNT–BZ ceramics were checked by X-ray diffraction machine (XRD, RAD III, Rigaku, Japan) using CuKα radiation (λ = 1.541 Å) at room temperature. The XRD patterns were collected in the Braggs–Brentano configuration operated at 10 mA and 20 kV with a step size of 0.02°. The particle size and shape was observed through field emission scanning electron microscope (FE-SEM, JP/JSM 5200, Japan). At room temperature, Raman scattering investigation was performed using a dispersive Raman spectrometer (ALMEGA, Nicelot, USA). Selected area electron diffraction (SAED) pattern and high-resolution transmission electron microscopy (HRTEM) images were obtained by transmission electron microscope (TEM) using a FE-TEM (JEOL/JEM-2100F version) operated at 200 kV. Both surfaces of the samples were polished and coated with a silver–palladium paste to form electrodes for electrical properties measurements. The dielectric constant and loss response were measured through an impedance analyzer (HP4194A, Agilent Technologies, Palo Alto, CA). The ferroelectric hysteresis loops were measured using a Precision Premier II device (Radiant Technology, Inc.) at 50 Hz. Field-induced strain response was measured using a contact-type displacement sensor (Model 1240; Mahr GmbH, Göttingen, Germany) at 50 mHz.

3. Results and discussion

Plate-like particles play a crucial role in the texture engineering. For texture development of BNT–BZ ceramics, plate-like BNT templates were first produced by a topochemical reaction from bismuth layered-structure ferroelectric (BLSF) BNT4 precursor through molten salt

http://dx.doi.org/10.5772/62688

process. **Figure 1** shows the crystalline phase and FE-SEM micrograph of BNT4 precursor particles synthesized by molten salt process. The X-ray diffraction pattern of the BNT4 precursor (**Figure 1a**) reveals the development of a single phase with no traces of secondary or parasite phases. All diffraction peaks inherit the characteristics features of the typical layered-perovskite structure. All diffraction peaks matches with the JCPDS card no. 74–1316 of the BLSF. Maximum number of peaks, for instance (006), (008), (0010), (0018), and (0020), were observed to possess higher intensities than the other peaks, signifying that the surface of BNT4 particles is parallel to the (00l) plane and suggesting that the BNT4 particles have high degree of preferred grain orientation. The FE-SEM micrograph of the BNT4 particles (**Figure 1b**) shows a plate-like morphology with size ranging from 15 to 20 μm. Some small grains of size less than one micron can be also observed that might be the broken pieces of BNT4 crystals. BNT4 has the characteristics anisotropic BLSF materials, in which the growth along the *a* and *b* axis is much higher than that of the c-axis. Thus, it is reasonable for them to adopt a plate-like morphology. The as-synthesized BNT4 particles produce in this work were used as a precursor materials for the TMC process [38].

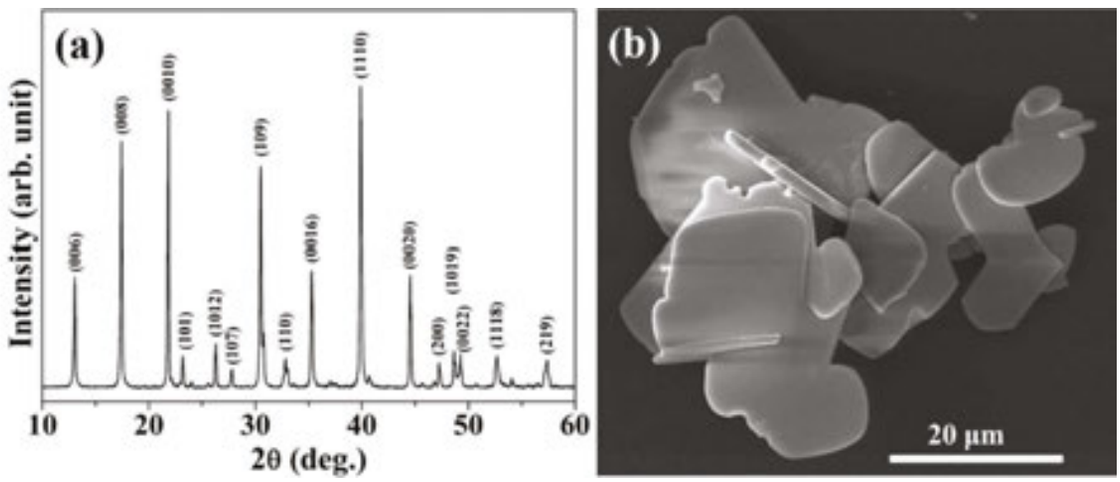

Figure 1. Crystal structure and FE-SEM micrograph of $Bi_{4.5}Na_{0.5}Ti_4O_{15}$ precursor particles synthesized by molten salt synthesis at 1150°C for 4 h (a) X-ray diffraction, (b) FE-SEM micrograph.

A schematic diagram showing the conversion of the layered perovskite into a simple perovskite structure by a topochemical conversion is illustrated in **Figure 2**. Bismuth layered-structure materials have a chemical formulation $Bi_2O_2(A_{m-1}B_mO_{3m+1})$ (where *A*-sites is occupied by Bi^{3+} and Na^+, while *B*-sites by Ti^{4+}, m is an integer with a certain value). For $m = 4$, the formula takes the form of $Bi_2O_2(Na_{0.5}Bi_{2.5})Ti_4O_{13}$ and this formula unit has the intergrowths of pseudo-perovskite blocks that are sandwiched between bismuth oxide layers. The BO_6 octahedron have a covalent linkage of $[Bi_2O_2]^{2+}$ among two-dimensional pseudo-perovskite layers. BNT4 belongs to the bismuth layered-structure compounds family, where Na^+ ions partially occupy the *A*-site. Na^+ could replace the $[Bi_2O_2]^{2+}$ slabs and the *A*-site (Bi^{3+} ions) during the topochemical reaction, where Bi_2O_3 forms and the weak covalent linkage of $[Bi_2O_2]^{2+}$ layer disappears. Furthermore, Na^+ ions substitute the Bi^{3+} ions in the *A*-site of the perovskite structure. More-

over, the tetragonal BNT4 transforms into a cubic BNT that preserves the morphological topographies of the precursor BNT4 [38].

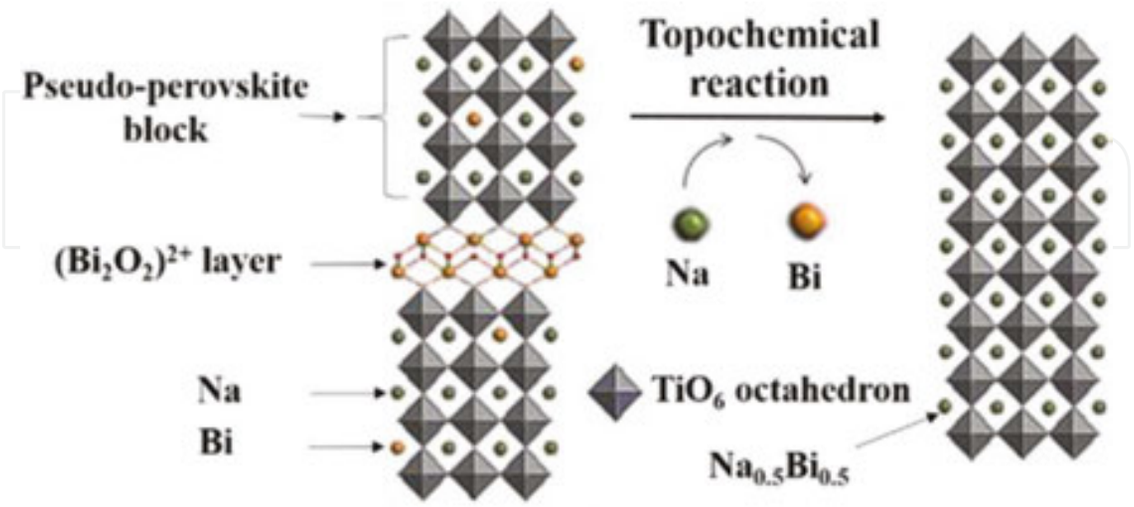

Figure 2. Schematic diagram of the conversion of layered-structure perovskite $Bi_{4.5}Na_{0.5}Ti_4O_{15}$ into a simple perovskite $Bi_{0.5}Na_{0.5}TiO_3$ by a topochemical microcrystal conversion. Reprinted with permission from Hussain et al. [38] with a copyright from Elsevier 2015.

Figure 3 presents the X-ray diffractogram of the BNT particles produced through TMC (**Figure 3a**) and CMO (**Figure 3b**) methods, respectively. BNT particles produced through both methods exhibit a single-phase perovskite structure and both match well with the JCPDS card No. 36–0340 of the $Bi_{0.5}Na_{0.5}TiO_3$. Because of the small rhombohedral distortion, all diffraction peaks were indexed on the basis of the pseudocubic perovskite unit cell. A significant difference in the peak intensities can be observed in BNT particles synthesized by two different routes. BNT particles synthesized by TMC shown in **Figure 3a** exhibit strong (100) and (200) diffraction peaks while that synthesized by CMO have (110) as major peak (shown in **Figure 3b**). This diffraction profile clearly indicate that the layered structure of BNT4 particles completely transformed into perovskite BNT templates after the TMC process (**Figure 3a**). Furthermore, the perovskite BNT preserves the plate-like morphology BNT4. Analogous to BNT4 templates, most of the large and plate-like BNT particles laid down with the c-axis aligned along the vertical direction during the sample preparation for the XRD analysis. Accordingly, they show strong diffraction peaks of (100) and (200). BNT4 belongs to the BLSFs family that possess $(Bi_{2.5}Na_{0.5}Ti_4O_{13})^{2-}$ (pseudo-perovskite layers) enclosed in $(Bi_2O_2)^{2+}$ fluorite layers where the *A*-site is co-occupied by Na^+ as well as Bi^{3+} in a Na/Bi ratio of 0.2. This conversion from the layered structure into a simple perovskite is composed of two stages: firstly, the transmission of Na^+ and Bi^{3+} through the perovskite layers; secondly, the transfiguration of $(Bi_2O_2)^{2+}$ fluorite layers into the perovskite phase. It has been also reported that this transformation implies a change from a lamellar phase to a perovskite phase [36]; nevertheless, the process involving the change of the $(Bi_2O_2)^{2+}$ layers to perovskite structure still needs further detailed investigations [38].

http://dx.doi.org/10.5772/62688

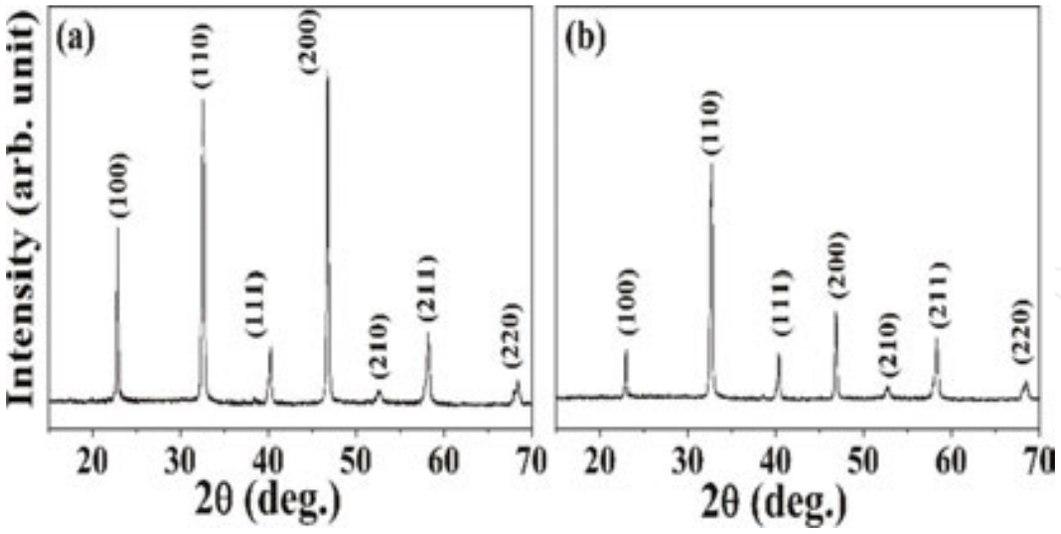

Figure 3. XRD diffraction of $Bi_{0.5}Na_{0.5}TiO_3$ particles synthesized by different methods (a) topochemical microcrystal conversion, (b) conventional mixed oxide route.

Figure 4 provides the FE-SEM micrographs of the BNT templates produced from the BNT4 precursor by TMC process along with the BNT particles prepared via a CMO route. Similar to BNT4 particles, most of the BNT templates have large grains of plate-like morphology. Such kind of large and plate-like particles are reasonably more suitable for the preparation textured ceramics by tape-casting process. Beside this, the BNT particles prepared by CMO possess small- and spherical-type grains. This kind of spherical grains is not appropriate to use as templates in development textured ceramics by RTGG technique. The EDS spectra of the BNT particles produced by TMC and CMO processes are displayed in **Figure 5**. This spectra clearly show the presence of Bi^{3+}, Na^{+}, Ti^{4+}, and O^{2-} ions in the particles, recommending successful synthesis of BNT particles through both processes. Additionally, the ratio of m_{Bi3+}:m_{Na}:m_{Ti4+}:m_{O2}− is close to the stoichiometric amount of the receptive BNT composition [38] in both cases.

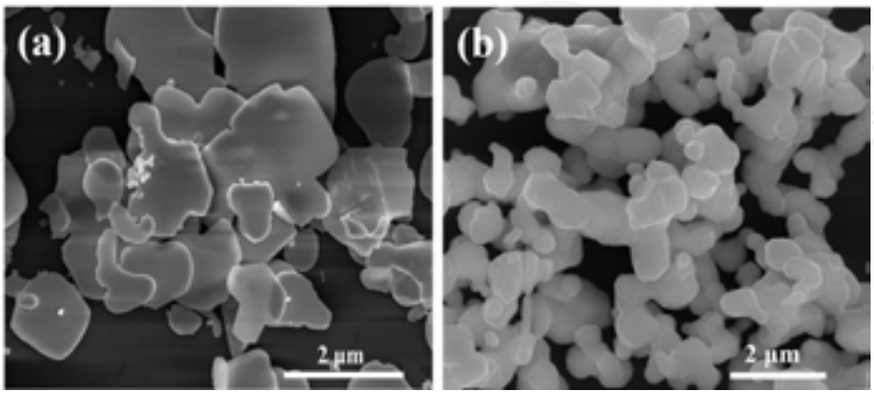

Figure 4. FE-SEM micrograph of $Bi_{0.5}Na_{0.5}TiO_3$ particles synthesized by different methods (a) topochemical microcrystal conversion, (b) conventional mixed oxide route. Reprinted with permission from Hussain et al. [38] with a copyright from Elsevier 2015.

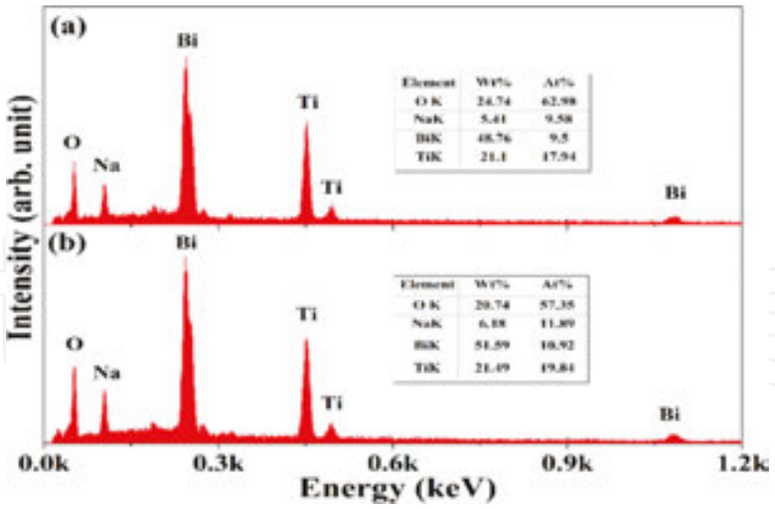

Figure 5. EDS spectrum of $Bi_{0.5}Na_{0.5}TiO_3$ particles synthesized by different methods (a) topochemical microcrystal conversion, (b) conventional mixed oxide route [38].

Figure 6 provides the Raman scattering spectra (in range 100–1000 cm^{-1}) of the polished surface of NBT particles measured at room temperature. The different vibration modes observed in Raman spectra of both sample is consistent with previously reported NBT-based ceramics [40–44]. The Raman-active mode (A_1) positioned around 150 cm^{-1} is associated with the *A*-site cations vibrations of the perovskite structure, which could be due to cations distortion or clusters of octahedral [BiO_6] and [NaO_6]. The peak around 270 cm^{-1} is attributed to the Ti–O vibrations, and the wavenumber in the range of 450–700 cm^{-1} often known as host modes is related to the TiO_6 octahedra vibrations, while high-frequency range over 700 cm^{-1} is due to

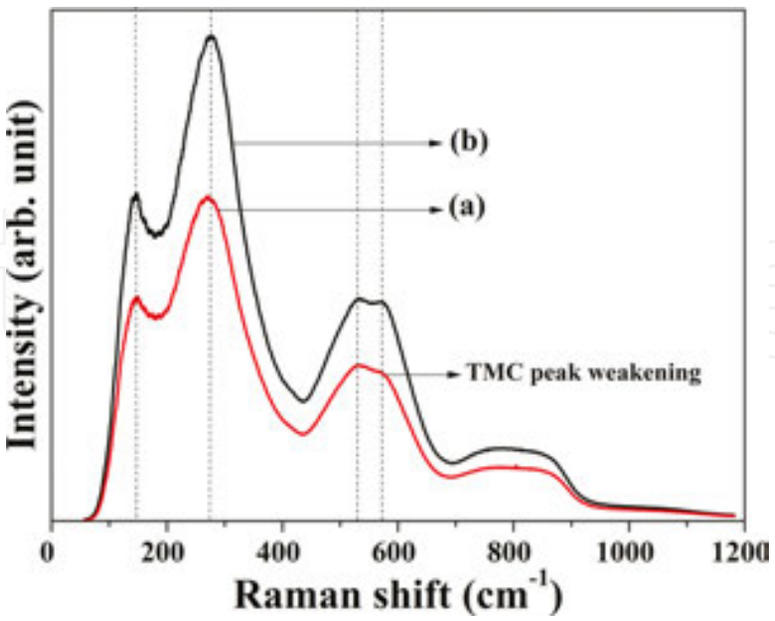

Figure 6. Raman scattering spectra of $Bi_{0.5}Na_{0.5}TiO_3$ particles synthesized by different methods (a) topochemical microcrystal conversion, (b) conventional mixed oxide route.

http://dx.doi.org/10.5772/62688

overlapping of A_1 (longitudinal optical) and E (longitudinal optical) bands. The NBT particles produced by TMC method show broadened and diffuse peaks around 270 cm^{-1} (Ti–O) and 450–700 cm^{-1} (TiO_6) vibration modes. It can be noted that the two individual TiO_6 octahedra vibration modes tend to diffuse, where the later mode centered around 550 cm^{-1} of the TMC-synthesized BNT sample exhibits weakening in intensity, which indicates the softening behavior in modes. Such phonon behavior suggests higher asymmetry in structure.

Figure 7 presents the TEM pictures of the BNT particles synthesized by TMC and CMO methods, respectively. The SEAD pattern of the BNT particles synthesized by TMC method shows dot pattern (**Figure 7a**), suggesting its single-crystal-type behavior, while that synthesized by CMO exhibits a ring-type configuration (**Figure 7b**) indicating a polycrystalline nature. The lattice spacing calculated from the HRTEM image (**Figure 7c**) of the TMC-synthesized BNT particles is 0.389 nm, which is consistent with the lattice spacing of the cubic (100) plane. This calculation suggests that TMC-synthesized BNT particles have a single-crystal nature and preferentially grow along the [100] direction which is further confirmed by the SAED pattern provided in (**Figure 7a**). Beside this, the lattice spacing of the CMO-synthesized BNT particles calculated from the HRTEM image (**Figure 7b**) is 0.275 nm; this value is consistent with the (110) plane lattice spacing of the BNT composition signifying a grain orientation of particles along [110] direction. These findings verify the XRD analysis of BNT particles synthesized by different routes. Therefore, the variation in microstructure along with the difference in lattice spacing of the CMO- and TMC-synthesized BNT particles indicates their successful fabrication [38].

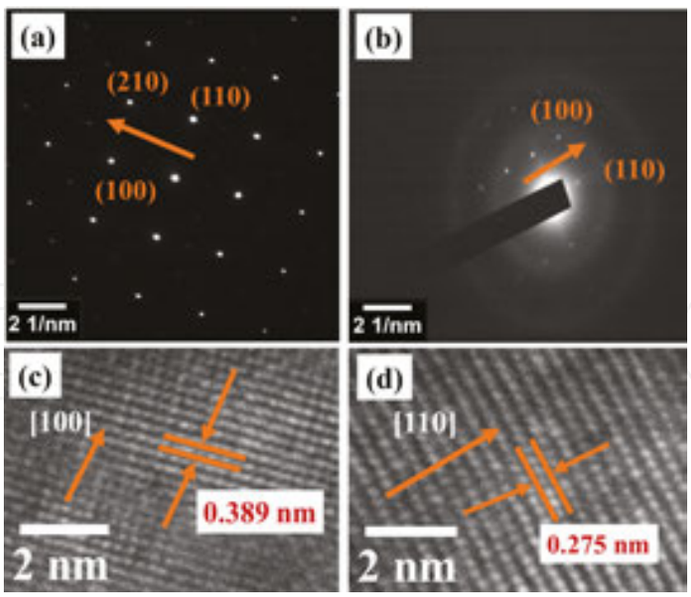

Figure 7. TEM images of $Bi_{0.5}Na_{0.5}TiO_3$ particles synthesized by different techniques (a) SAED pattern of $Bi_{0.5}Na_{0.5}TiO_3$ particles synthesized by topochemical microcrystal conversion method, (b) SAED pattern of $Bi_{0.5}Na_{0.5}TiO_3$ particles synthesized by conventional mixed oxide route, (c) HRTEM image of $Bi_{0.5}Na_{0.5}TiO_3$ particles synthesized by topochemical microcrystal conversion method, (d) HRTEM image of $Bi_{0.5}Na_{0.5}TiO_3$ particles synthesized by conventional mixed oxide route Reproduced from reference [38] with a copyright from Elsevier 2015.

The BNT particles synthesized by TMC method were further utilized as templates for texture development of BNT–BZ ceramics. **Figure 8** shows a schematic diagram for the development of textured BNT–BZ ceramics by tape-casting method. A green sheet of a thickness about 100 μm was formed on SiO_2-coated polyethylene film through a doctor blade technique, and 25 different green sheets were laminated and hot-pressed to develop a thick green compact of about 2 mm. The green compacts were then sintered to measure their structural and electromechanical properties.

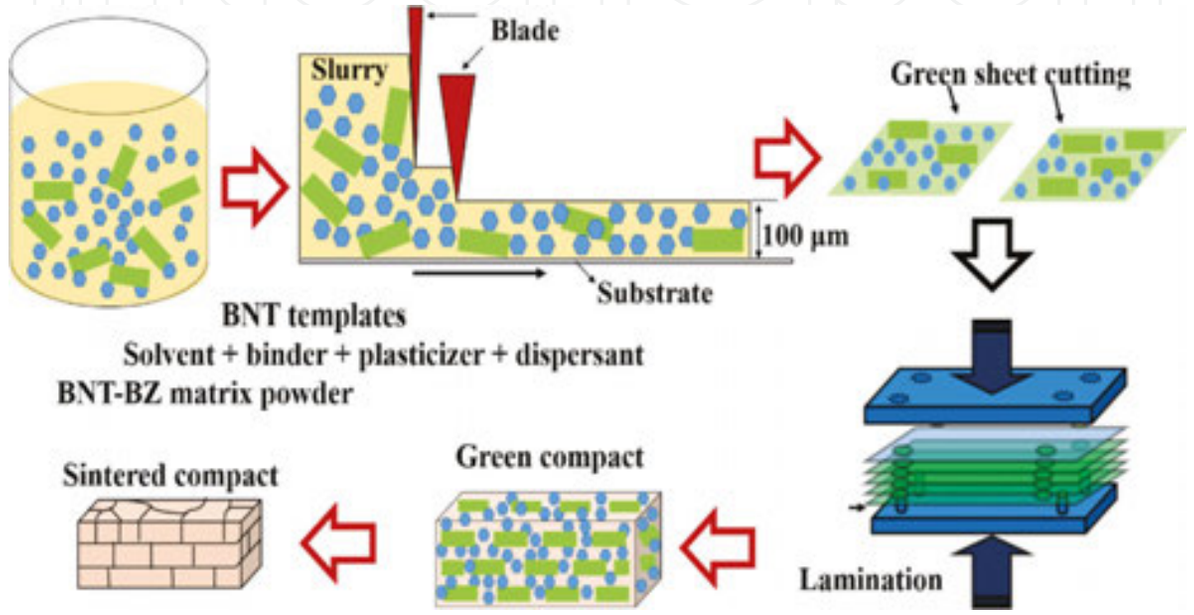

Figure 8. Schematic diagram of the textured BNT–BZ ceramics produced by RTGG method.

Figure 9a, b provides a comparison of the XRD pattern of the textured and non-textured BNT–BZ ceramics. For texture development of BNT–BZ ceramics, 15 wt% BNT templates were used as seed particles. The diffraction pattern of both samples display a single-phase perovskite structure**.** Textured sample (**Figure 9a**) produced by RTGG process shows (100) and (200) peaks much higher than that of the corresponding non-texture sample, suggesting a preferred grain orientation. The non-textured ceramic (**Figure 9b**) produced by conventional method shows a strong (110) diffraction peak indicating a random orientation. The overall comparison shows that the textured ceramics exhibit [100] diffraction peak dominant, indicating that a large fraction of grains are aligned with their *a*-axis normal to the sample surface. The degree of grain orientation was estimated by the Lotgering factor (F), which is given by

$$F = \frac{P - P_o}{1 - P_o}$$

Where

http://dx.doi.org/10.5772/62688

$$P = \frac{\sum I(h00)}{\sum I(hkl)}, P_o = \frac{\sum I_o(h00)}{\sum I_o(hkl)}$$

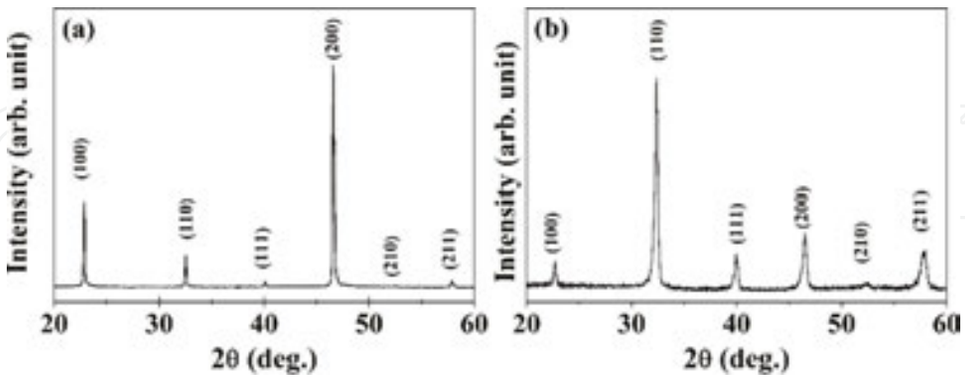

Figure 9. XRD pattern of the BNT–BZ ceramics (a) textured sample, (b) non-textured sample.

where I and I_o are the relative intensity of the diffraction peaks of the textured and non-textured ceramics, respectively, and (h00) and (hkl) are their miller indices. The degree of grain orientation obtained by the method is not very accurate due to the intensity of the diffraction peaks from which the slightly misaligned grains are not counted in the measurement of $I_{(h00)}$ and $I_{(hkl)}$. However, the F values are used in this work because of their convenience in the measurements. The F values vary from zero for a randomly oriented sample, to one, for a completely oriented sample. The F values were calculated from the diffraction peaks lies in the 2θ range from 20° to 70°. A high Lotgering factor F about 0.83 was obtained for the textured BNT–BZ sample, signifying a high degree of preferred grain orientation. This result also indicates that the plate-like BNT templates are proficient in prompting grain orientation in the BNT–BZ ceramics. Previously, Tam et al. [45] utilized (20 wt%) BNT templates for $Bi_{0.5}Na_{0.35}K_{0.1}Li_{0.05}TiO_3$ (BNKLT) ceramics and reported a Lotgering factor of 0.6. The results obtained in this work indicate that the present high-quality BNT template by TMC process has the potential to develop oriented ceramics with enhanced grain orientation factor in regular perovskite-type ceramics. Moreover, high grain orientation factor of the textured BNT–BZ ceramics usually improves the piezoelectric properties in comparison with the non-textured sample of the same material [38].

The temperature dependence of the dielectric constant (ε) and loss (tanδ) of the textured and non-textured BNT–BZ ceramics measured at different frequencies (1, 10, and 100 kHz) is shown in **Figure 10**. Both samples show increase in dielectric constant with increase in temperature up to certain value and then decrease with further increase in temperature. At all measured frequencies, textured sample exhibits two visible diffuse dielectric anomalies, termed as a depolarization temperature (T_d) appeared at 140°C along with a permittivity maximum temperature (T_m) around 280°C. Nevertheless, the T_d anomaly is not visible in the dielectric curves of the non-textured specimen and its T_m values are lower than that of the textured sample. The fading of T_d anomaly in the non-textured specimen signifies the weakening of the ferroelectric phase and formation of the relaxor phase as reported previously for

BNT–BZ system [44]. The dielectric constant measured at room temperature increased from 1200 for the non-texture sample to 1500 for the textured sample. Furthermore, the dielectric loss of the textured sample is slightly higher than that of non-textured sample, probably due to its lower density and defects/impurities introduced into the green laminates during the tape-casting process.

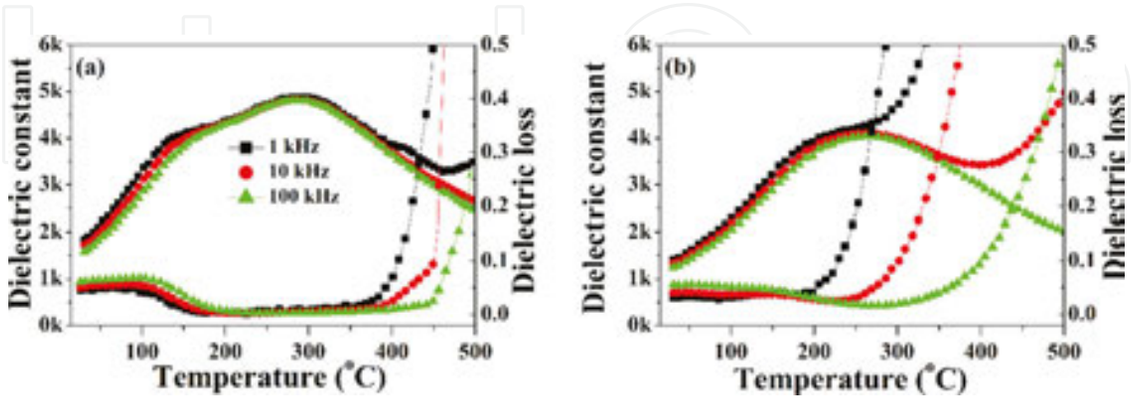

Figure 10. Dielectric constant and loss of BNT–BZ ceramics (a) textured sample, (b) non-textured sample.

Figure 11a, b shows the room temperature P–E hysteresis loops of the textured and non-textured BNT–BZ ceramics measured at 50 Hz. The textured sample (**Figure 11a**) exhibits a pinch-type P–E loop, while the non-textured sample (**Figure 11b**) exhibits a slim at an applied field of 70 kV/cm. Moreover, texture development improved the ferroelectric response of the BNT–BZ ceramics. The remnant and maximum polarization at an electric field of 70 kV/cm, respectively, increased from 5 and 26 μm/cm^2 for non-textured sample to 11 and 35 μm/cm^2

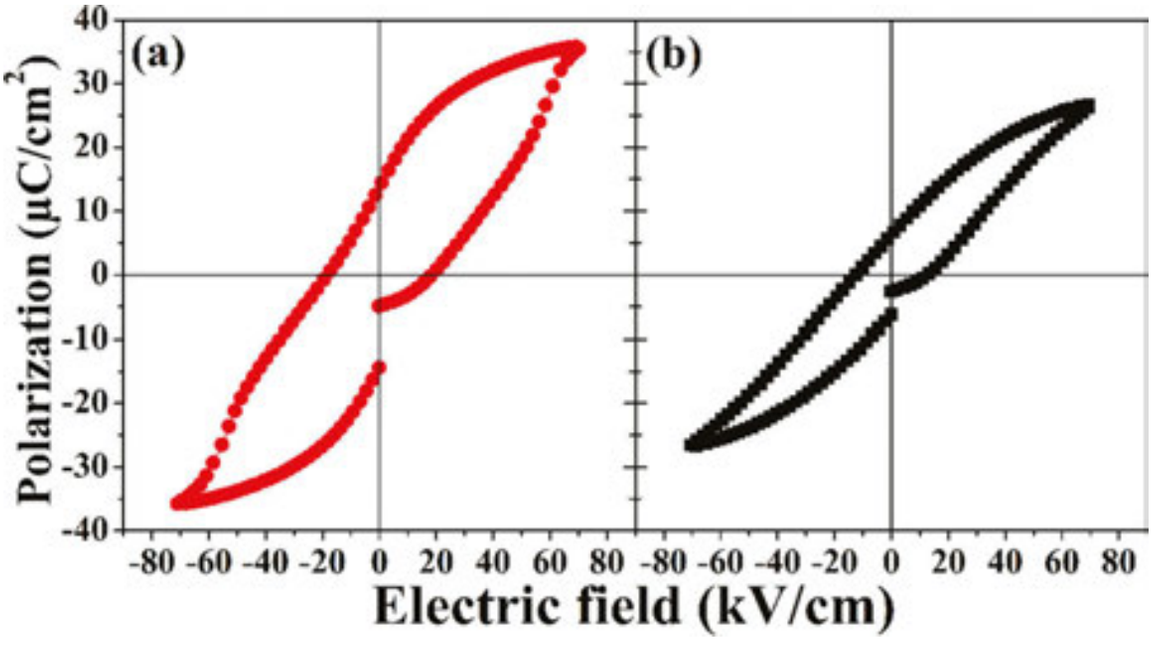

Figure 11. Ferroelectric response of BNT–BZ ceramics (a) textured sample, (b) non-textured sample.

http://dx.doi.org/10.5772/62688

for it textured counterpart. The coercive field (E_c) increased from 13 kV/cm for the non-textured sample to 18 kV/cm for the textured sample. This enhancement in the polarization can be associated with the crystallographic grain orientation of the textured sample.

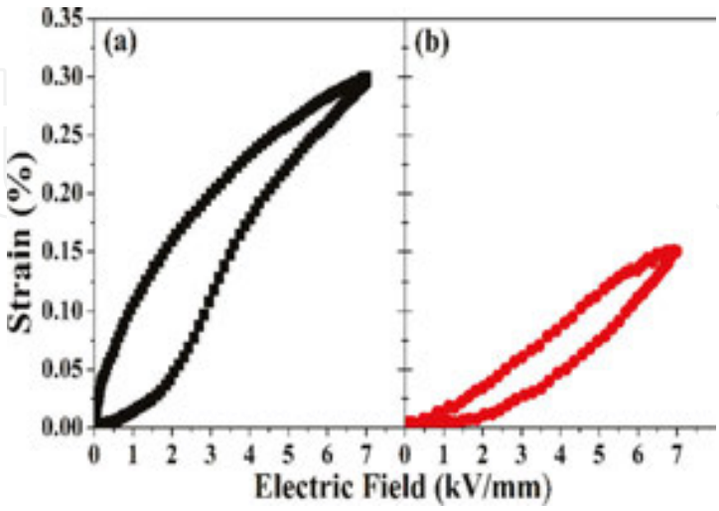

Figure 12. Unipolar field-induced strain response of BNT–BZ ceramics (a) textured sample, (b) non-textured sample. Reproduced from reference [38] with a copyright from Elsevier 2015.

	Relative density	ε	**Strain**	d^*_{33}
Textured	93%	1500	0.30%	428 pm/V
Non-textured	96%	1200	0.15%	214 pm/V
Increase	-	25%	100%	100%

Reprinted with permission from Hussain et al. [38] with a copyright from elsewhere 2015.

Table 1. Dielectric and piezoelectric properties of textured and non-textured BNT–BZ ceramics.

The field-induced unipolar strain of the textured and non-textured BNT–BZ ceramics was examined at an applied electric field of 70 kV/cm and is shown in **Figure 12**. The overall field-induced strain response of textured specimen (**Figure 12a**) is higher than that of the non-textured sample (**Figure 12b**). The unipolar field-induced strain level raised from 0.15% for the non-textured sample to 0.30% for the textured sample. The corresponding normalized strain ($d^*_{33} = S_{max}/E_{max}$) obtained for these specimens are 214 and 428 pm/V, respectively. **Table 1** provides the density, dielectric, and piezoelectric response of the textured and non-textured BNT–BZ samples at room temperature. The comparison of both specimens clearly shows that textured ceramics have a better electromechanical properties than non-textured counterparts. The dielectric constant measured at room temperature increased from 1200 to 1500, while the unipolar field-induced strain level enhanced from 0.15 to 0.30% for the non-textured and textured samples, respectively. This is almost 25 and 100% enhancement after texturing process. This increase in dielectric and field-induced strain response can be attributed to the

(100) preferred orientation developed by plate-like BNT templates. The results obtained from the BNT–BZ ceramics evidently show that texture development significantly improve the electromechanical properties of the BNT–BZ ceramics and enable them as promising lead-free candidates in piezoelectric industry.

4. Summary

For texture development of $BaZrO_3$-modified $Bi_{0.5}Na_{0.5}TiO_3$ (BNT–BZ) ceramics, plate-like $Bi_{0.5}Na_{0.5}TiO_3$ (BNT) template was first synthesized from bismuth layer-structured ferroelectric $Bi_{4.5}Na_{0.5}Ti_4O_{15}$ (BNT4) precursor through a TMC method. The BNT template produced by TMC method presented high aspect ratio plate-like grains that inherit the morphology of the BNT4 precursor particles and are different from the CMO-synthesized BNT particles that exhibit round-type grains of submicron size. The TMC-synthesized BNT particles show strong (*h*00) intensity peaks signifying (100) preferred grain orientation; however, the CMO-synthesized particles exhibit (110) intense peak, revealing a random orientation. The structural characteristics observed in XRD analysis further inveterate the TEM analysis, verifying the grain growth along (100) plane for TMC process and along (110) plane for the same BNT composition produced through CMO route. The BNT templates produced by TMC process are very effective in the texture engineering of BNT–BZ ceramics. A high Lotgering factor (F = 83%) was observed in BNT–BZ ceramics textured with 15 wt% of BNT templates. Furthermore, room temperature dielectric constant increased by 25%, maximum polarization 34%, and field-induced strain response by 100%. The results obtained in this work shows that BNT templates play an important role in the texture engineering of BNT–BZ ceramics and improving the dielectric, ferroelectric, and field-induced strain properties.

Acknowledgements

This work is supported by the National Research Foundation of Korea (NRF) grant funded by the Korean government (MOE) (2013R1A1A2058345) and the Basic Research program through the National Research Foundation of Korea (NRF) funded by Ministry of Education, Science and Technology (MEST) (2011–0030058).

Author details

Ali Hussain* and Myong-Ho Kim

*Address all correspondence to: alihussain_phy@yahoo.com

School of Advanced Materials Engineering, Changwon National University, Gyeongnam, Republic of Korea

References

[1] Jaffe B, Cook WR, Jaffe H: Piezoelectric ceramics. Academic Press: London, UK 1971. doi:10.1016/0022-460X(72)90684-0

[2] Haertling GH: Ferroelectric ceramics: History and technology. J. Am. Ceram. Soc. 1999; 82(4): 797–818. doi:10.1111/j.1151-2916.1999.tb01840.x

[3] Jeong CK, Lee J, Han S, Ryu J, Hwang GT, Park DY, Park JH, Lee SS, Byun M, Ko SH, Lee KJ: A hyper-stretchable elastic-composite energy harvester. Adv. Mater. 2015; 27: 2866–2875. doi:10.1002/adma.201500367

[4] Setter N: Piezoelectric materials in devices: Extended reviews on current and emerging piezoelectric materials, technology, and applications. EPFL Swiss Federal Institute of Technology: Lausanne, Switzerland, 2002. ISBN: 2970034603, 9782970034605

[5] Vijaya MS: Piezoelectric materials and devices: Applications in engineering and medical sciences. CRC Press Taylor & Francis Group New York, 2013. ISBN: 13: 978-1-4398-8788-2.

[6] EU-directive 2002/95/EC: Restriction of the use of certain hazardous substances in electrical and electronic equipment (RoHS). Off. J. Eur. Union. 2003; 46: 19–23.

[7] EU-directive 2002/96/EC: Waste electrical and electronic equipment (WEEE). Off. J. Eur. Union. 2003; 46: 24–38.

[8] US California Senate. Bill No. 20: Solid waste: Hazardous electronic waste 2003; Chapter 256: 1–19.

[9] Park Y, Cho K, Kim HG: Effect of external pressure and grain size on the phase transition in the Gd-doped $BaTiO_3$ ceramic. Mater. Res. Bull. 1997; 32: 1485–1494. doi: 10.1016/S0025-5408(97)00130-X

[10] Lacourse Brain C, Vasantha-Amarakoon RW: Characterization of firing schedule for positive temperature coefficient of resistance $BaTiO_3$. J. Am. Ceram. Soc. 1995; 78: 3352–3356. doi:10.1111/j.1151-2916.1995.tb07976.x

[11] Jona F, Shirane G: Ferroelectric crystals, Dover Publications, INC.: New York, 1993. ISBN-13: 978–0486673868

[12] Koelzynski A, Tkacz-Smiech K: From the molecular picture to the band structure of cubic and tetragonal barium titanate. Ferroelectrics. 2005; 314: 123–134. doi: 10.1080/00150190590926300

[13] Egerton L, Dillon DM: Piezoelectric and dielectric properties of ceramics in the system potassium-sodium niobate. J. Am. Ceram. Soc. 1959. 42; 438–42. doi:10.1111/j. 1151-2916.1959.tb12971.x

[14] Cross LE: Electric double hysteresis in $(K_xNa_{1-x})NbO_3$ single crystals. Nature. 1958; 181: 178–179. doi:10.1038/181178a0

[15] Jeager RE, Egerton L: Hot pressing of potassium–sodium niobates. J. Am. Ceram. Soc. 1962; 45: 209–213. doi:10.1111/j.1151-2916.1962.tb11127.x

[16] Haertling GH, Properties of hot-pressed ferroelectric alkali niobate ceramics. J. Am. Ceram. Soc. 1967; 50: 329–330. doi:10.1111/j.1151-2916.1967.tb15121.x

[17] Hollenstein E, Davis M, Damjanovic D, Setter N: Piezoelectric properties of Li- and Ta-modified $(K_{0.5}Na_{0.5})NbO_3$ ceramics. Appl. Phys. Lett. 2005; 87: 182905–3. doi: 10.1063/1.2123387

[18] Saito Y, Takao H, Tani T, Nonoyama T, Takatori K, Homma T, Nagaya T, Nakamura M: Lead-free piezoceramics. Nature. 2004; 432: 84–87. doi:10.1038/nature03028

[19] Eerd BW, Damjanovic D, Klein N, Setter N, Trodahl J: Structural complexity of $(Na_{0.5}Bi_{0.5})TiO_3$–$BaTiO_3$ as revealed by Raman spectroscopy. Phys. Rev. B. 2010; 82: 104112–104117. doi:10.1103/PhysRevB.82.104112

[20] Dittmer R., Webber KG, Aulbach E, Jo W, Tan X, Rdel J: Electric-field-induced polarization and strain in $0.94(Bi_{1/2}Na_{1/2})TiO_3$–$0.06BaTiO_3$ under uniaxial stress. Acta Mater. 2013; 61: 1350–1358. doi:10.1016/j.actamat.2012.11.012

[21] Zhang ST, Kounga AB, Aulbach E, Ehrenberg H, Rdel J: Giant strain in lead-free piezoceramics $Bi_{0.5}Na_{0.5}TiO_3$–$BaTiO_3$–$K_{0.5}Na_{0.5}NbO_3$ system. Appl. Phys. Lett. 2007; 91: 112906–3. doi:10.1063/1.2783200

[22] Hiruma Y, Nagata H, Takenaka T: Detection of morphotropic phase boundary of $(Bi_{1/2}Na_{1/2})TiO_3$–$Ba(Al_{1/2}Sb_{1/2})O_3$ solid-solution ceramics. Appl. Phys. Lett. 2009; 95: 052903. doi:10.1063/1.3194146

[23] Tani T: Crystalline-oriented piezoelectric bulk ceramics with a perovskite-type structure. J. Korean Phys. Soc. 1998; 32: S1217–S1220. doi:10.3938/jkps.32.1217

[24] Messing GL, McKinstry ST, Sabolsky EM, Duran C, Kwon S, Brahmaroutu B, Park P, Yilmaz H, Rehrig PW, Eitel KB, et al.: Templated grain growth of textured piezoelectric ceramics. Crit. Rev. Solid State Mater. Sci. 2004; 29: 45–96. doi: 10.1080/10408430490490905

[25] Kimura T, Takahashi T, Tani T, Saito Y: Crystallographic texture development in bismuth sodium titanate prepared by reactive-templated grain growth method. J. Am. Ceram. Soc. 2004; 87: 1424–1429. doi:10.1111/j.1551-2916.2004.01424.x

[26] Malik RA, Kang J, Hussain A, Ahn CW, Han H, Lee J: High strain in lead-free Nb-doped $Bi_{1/2}(Na_{0.84}K_{0.16})_{1/2}TiO_3$–$SrTiO_3$ incipient piezoelectric ceramics. Appl. Phys. Express. 2014; 7: 061502–4. doi:10.7567/APEX.7.061502

[27] Rödel J, Webber K, Dittmer R, Jo W, Kimura M, Damjanovic D: Transferring lead-free piezoelectric ceramics into application. J. Eur. Ceram. Soc. 2015; 35: 1659–1681. doi: 10.1016/j.jeurceramsoc.2014.12.013

[28] Chang YF, Poterala SF, Yang ZP, Mckinstry ST, Messing GL: ⊚001⊚ textured $(K_{0.5}Na_{0.5})(Nb_{0.97}Sb_{0.03})O_3$ piezoelectric ceramics with high electromechanical coupling over a broad temperature range. Appl. Phys. Lett. 2009; 95: 232905–3. doi:10.1063/1.3271682

[29] Kimura T: Application of texture engineering to piezoelectric ceramics. J. Ceram. Soc. Jpn. 2006; 114: 15–25.

[30] Przybylski K, Brylewski T, Bucko M, Prażuch J, Morawski A, Łada T: Synthesis and properties of superconducting (Hg,Re)–Ba–Ca–Cu–O thick films on polycrystalline $LaAlO_3$ substrate obtained by screen-printing method. Phys. C. 2003; 387: 225–229. doi: 10.1016/S0921-4534(03)00675-0

[31] Wu M, Li Y, Wang D, Zeng J, Yin Q: ABS-064: Grain oriented $(Na_{0.5}Bi_{0.5})_{0.94}Ba_{0.06}TiO_3$ piezoceramics prepared by the screen-printing multilayer grain growth technique. J. Electroceram. 2009; 22: 131–135. doi:10.1007/s10832-007-9392-z

[32] Sun S, Pan X, Wang P, Zhu L, Huang Q, Li D, Yin Z: Fabrication and electrical properties of grain-oriented $0.7Pb(Mg_{1/3}Nb_{2/3})O_3$–$0.3PbTiO_3$ ceramics. Appl. Phys. Lett. 2004; 84: 574–576. doi:10.1063/1.1643537

[33] Hussain A, Ahn CW, Lee JH, Kim IW, Lee JS, Jeong, SJ, Rout SK: Anisotropic electrical properties of $Bi_{0.5}(Na_{0.75}K_{0.25})_{0.5}TiO_3$ ceramics fabricated by reactive templated grain growth (RTGG). Curr. Appl. Phys. 2010; 10: 305–310. doi:10.1016/j.cap.2009.06.013

[34] Takao H, Saito Y, Aoki Y, Horibuchi K: Microstructural evolution of crystalline-oriented $(K_{0.5}Na_{0.5})NbO_3$ piezoelectric ceramics with a sintering aid of CuO. J. Am. Ceram. Soc. 2006; 89: 1951–1956. doi:10.1111/j.1551-2916.2006.01042.x

[35] Seabaugh MM, Kerscht IH, Messing GL: Texture development by templated grain growth in liquid-phase-sintered α-Alumina. J. Am. Ceram. Soc. 1997; 80: 1181–1188. doi:10.1111/j.1151-2916.1997.tb02961.x

[36] Raymond ES, Thomas EM: Topochemical synthesis of three dimensional perovskites from lamellar precursors. J. Am. Chem. Soc. 2000; 122: 2798–2803. doi:10.1021/ja993306i

[37] Borg S, Svensson G, Bovinw J: Structure study of $Bi_{2.5}Na_{0.5}Ta_2O_9$ and $Bi_{2.5}Na_{m\text{-}1.5}Nb_mO_3$ (m (2–4)) by neutron powder diffraction and electron microscopy. J. Solid State Chem. 2002; 167: 86–96. doi:10.1006/jssc.2002.9623

[38] Hussain A, Rahman JU, Ahmed F, Kim JS, Kim MH, Song TK, Kim WJ: Plate-like $Na_{0.5}Bi_{0.5}TiO_3$ particles synthesized by topochemical microcrystal conversion method. J. Eur. Ceram. Soc. 2015; 35: 919–925. doi:10.1016/j.jeurceramsoc.2014.10.004

[39] Rahman JU, Hussain A, Maqbool A, Song TK, Kim WJ, Kim SS, et al.: Dielectric, ferroelectric and field-induced strain response of lead-free $BaZrO_3$-modified

$Bi_{0.5}Na_{0.5}TiO_3$ ceramics. Curr. Appl. Phys. 2014; 14: 331–336. doi:10.1016/j.cap.2013.12.009

[40] Chen C, Zhang H, Deng H, Huang T, Li X: Electric field and temperature-induced phase transition in Mn-doped $Na_{1/2}Bi_{1/2}TiO_3$-5.0 at.%$BaTiO_3$ single crystals investigated by micro-Raman scattering. Appl. Phys. Lett. 2014; 104: 142902–5. doi:10.1063/1.4870504

[41] Luo L, Ge W, Li J, Viehald D, Farley C, Bondr R: Raman spectroscopic study of $Na_{1/2}Bi_{1/2}TiO_3$–x%$BaTiO_3$ single crystals as a function of temperature and composition. J. Appl. Phys. 2011; 109: 113507–6. doi:10.1063/1.3587236

[42] Parija B, Rout SK, Cavalcante LS, Simoes AZ, Panigrahi S, Longo E, Batista NC: Structure, microstructure and dielectric properties of 100-x($Bi_{0.5}Na_{0.5}$)TiO_3–x[$SrTiO_3$] composites ceramics. Appl. Phys. A. 2012; 109: 715–723. doi:10.1007/s00339-012-7105-1

[43] Hussain A, Rahman JU, Maqbool A, Kim MS, Song TK, Kim WJ, Kim MH: Structural and electromechanical properties of lead-free $Na_{0.5}Bi_{0.5}TiO_3$–$BaZrO_3$ ceramics. Phys. Status Solidi A. 2014; 211: 1704–1708. doi:10.1002/pssa.201330472

[44] Maqbool A, Hussain A, Rahman JU, Song TK, Kim WJ, Lee J, Kim MH: Enhanced electric field-induced strain and ferroelectric behavior of ($Bi_{0.5}Na_{0.5}$)TiO_3–$BaTiO_3$–$SrZrO_3$ lead-free ceramics. Ceram. Int. 2014; 40: 11905–11914. doi:10.1016/j.ceramint.2014.04.026

[45] Tam W, Kwok K, Zeng J, Chan H: Fabrication of textured BNKLT ceramics by reactive templated grain growth using NBT templates. J. Phys. D Appl. Phys. 2008; 41: 045402–4. doi:10.1088/0022-3727/41/4/045402